Enhanced chiral response from the Fabry–Perot cavity coupled meta-surfaces*

Ze-Jian Yang(阳泽健)[1,2], De-Jiao Hu(胡德骄)[1,2], Fu-Hua Gao(高福华)[1,2,†], and Yi-Dong Hou(侯宜栋)[1,2]

[1] College of Physical Science and Technology, Sichuan University, Chengdu 610064, China
[2] Sino-British Joint Materials Research Institute, Sichuan University, Chengdu 610064, China

(Received 2 February 2016; revised manuscript received 5 April 2016; published online 25 June 2016)

The circular dichroism (CD) signal of a two-dimensional (2D) chiral meta-surface is usually weak, where the difference between the transmitted (or reflected) right and left circular polarization is barely small. We present a general method to enhance the reflective CD spectrum, by adding a layer of reflective film behind the meta-surface. The light passes through the chiral meta-surface and propagates towards the reflector, where it is reflected back and further interacts with the chiral meta-surface. The light is reflected back and forth between these two layers, forming a Fabry–Perot type resonance, which interacts with the localized surface plasmonic resonance (LSPR) mode and greatly enhances the CD signal of the light wave leaving the meta-surface. We numerically calculate the CD enhancing effect of an L-shaped chiral meta-surface on a gold film in the visible range. Compared with the single layer meta-surface, the L-shaped chiral meta-surface has a CD maximum that is dramatically increased to 1. The analysis of reflection efficiency reveals that our design can be used to realize a reflective circular polarizer. Corresponding mode analysis shows that the huge CD originates from the hybrid mode comprised of FP mode and LSPR. Our results provide a general approach to enhancing the CD signal of a chiral meta-surface and can be used in areas like biosensing, circular polarizer, integrated photonics, etc.

Keywords: chiral meta-surfaces, hybridization, Fabry–Perot resonance

PACS: 42.25.Bs, 42.25.Ja **DOI:** 10.1088/1674-1056/25/8/084201

1. Introduction

Chirality is a fundamental and ubiquitous property of natural materials and biomolecules, which, in a two-dimensional (2D) case, refers to the phenomenon that a structure cannot be superimposed into its mirror image without turning the structure over. In the last decade, chiral plasmonics has aroused a considerable research interest for its importance in the fields like polarization control,[1–12] negative metamaterials,[13] biosensing,[14] repulsive Casimir force,[15] etc. Novel electromagnetic properties have been realized due to the large chiral response in these plasmonic applications, such as asymmetric transmission,[4] broadband circular polarization conversion,[12] attomolar limit of detection for DNA,[14] and nondispersive optical activity.[16] The strength of chirality can be measured with the circular dichroism (CD) spectrum, which is usually the difference in transmission efficiency between left (LCP) and right circular polarized (RCP) incident light. However, the chirality strengths of natural materials are very weak. The progress of research in plasmonic and nanofabrication technique allows us to realize artificial chiral materials that are so-called chiral meta-materials (CMMs),[1–17] whose chiral effects are much higher than those of natural materials. Previously proposed structures can be divided into two types, the first type of structure is the 2D structure, including dual-layer twisted-layers,[1,2] multilayer gammadions,[3] U-shaped split ring resonators,[4,5] nonchiral square arrays,[6,7] etc. The second type of structure is the three-dimensional (3D) structure, such as metal-doped platinum clusters,[8] helical metamaterial,[9–11] and complex colloids.[12] Among the above devices, the 3D chiral structure has larger CD response, however, is difficult to fabricate and hard to use in the frequency range from visible to ultraviolet band. On the contrary, the 2D structure can be realized in an easier way. Giant CD has been achieved by layers of 2D CMMs which can act as a circular polarizer.[6] However, the CD of single meta-surface is usually not strong enough to satisfy the requirements for the polarization control. Methods have been presented to achieve stronger CD. To the best of our knowledge, giant CD has been achieved in double layer CMMs or the achiral metal squares with non-normal incidence.[5–7,13] The fabrication of double layer or multilayer CMMs requires more precise alignment and complicated process technology. As for the achiral meta-materials, working at oblique incidence is not always convenient experimentally. Beyond this, the single layer CMM with giant CD is usually in the near infrared region.[17]

In this paper, we present a general approach to enhancing the CD signal from a 2D single CMM by adding a reflector layer behind the CMM, which is composed of periodic L-shaped meta-atoms in our case. The localized surface plasmonic resonance (LSPR) supported by the meta-atoms gives

*Project supported by the National Natural Science Foundation of China (Grant No. 61377054).
†Corresponding author. E-mail: gaofuhua@scu.edu.cn
© 2016 Chinese Physical Society and IOP Publishing Ltd

rise to the reflection difference between the RCP and LCP, where this effect is further amplified by the Fabry–Perot (FP) resonance formed between the two layers. Numerical results show that the CD maximum of the reflected light is enhanced by nine times compared with that of the single layer meta-atoms in the visible optical range. Further analysis of reflection efficiencies demonstrates that only one polarization component (RCP to RCP) exists near the resonance wavelength, indicating that a circular polarizer is realized which can reflect one circular polarization without changing its handedness and absorb the other. The analysis of relevant modes and detailed influence of the layer separation proves that the enhancement of the CD signal originates from the hybrid mode, which comprises the FP and the LSPR. Furthermore, the influence of the periodicity is also investigated. Our results present an easy and practical method to enhance the CD signal from single layer CMMs and to realize a reflective circular polarizer, which can find its applications in integrated photonics and biosensing. Particularly, wave propagation in Fabry–Perot cavity presents a spin-dependent splitting.[18] Additionally, the spin-dependent displacements between the chiral metamaterials can be enhanced at certain incident angles.[19] Combining the above advantages, the chiral effect in the Fabry–Perot cavity may provide a possible way to enhance the photonic spin Hall effect.

2. Results and discussion

2.1. Enhanced CD

Figure 1(a) shows the schematic of the designed structure, where a periodic array of L-shaped CMM is located on the surface of a dielectric spacer (thickness t_2), underneath which is a layer of metallic reflector and the substrate. Due to the thick gold reflector, the transmittance of the whole system is totally zero. The spacer and the substrate are of SiO_2 with a refraction index of 1.46. The L-shaped meta-atoms are featured by arm lengths L_x and L_y, width W, and thickness t_1. The lattice spacings between two meta-atoms are d_x and d_y. The optical response of the structure is calculated by using a commercial software package (Lumerical) based on the finite difference time domain (FDTD) method. The geometric parameters used in the simulation are $L_x = 120$ nm, $L_y = 240$ nm, $W = 80$ nm, $t_1 = 50$ nm, $t_2 = 335$ nm, $t_3 = 200$ nm, $d_x = 120$ nm, and $d_y = 240$ nm. The CMM and reflector layers are made of gold, whose permeability is 1 and permittivity is cited from the literature.[20] The light normally illuminates the CMM and is reflected later.

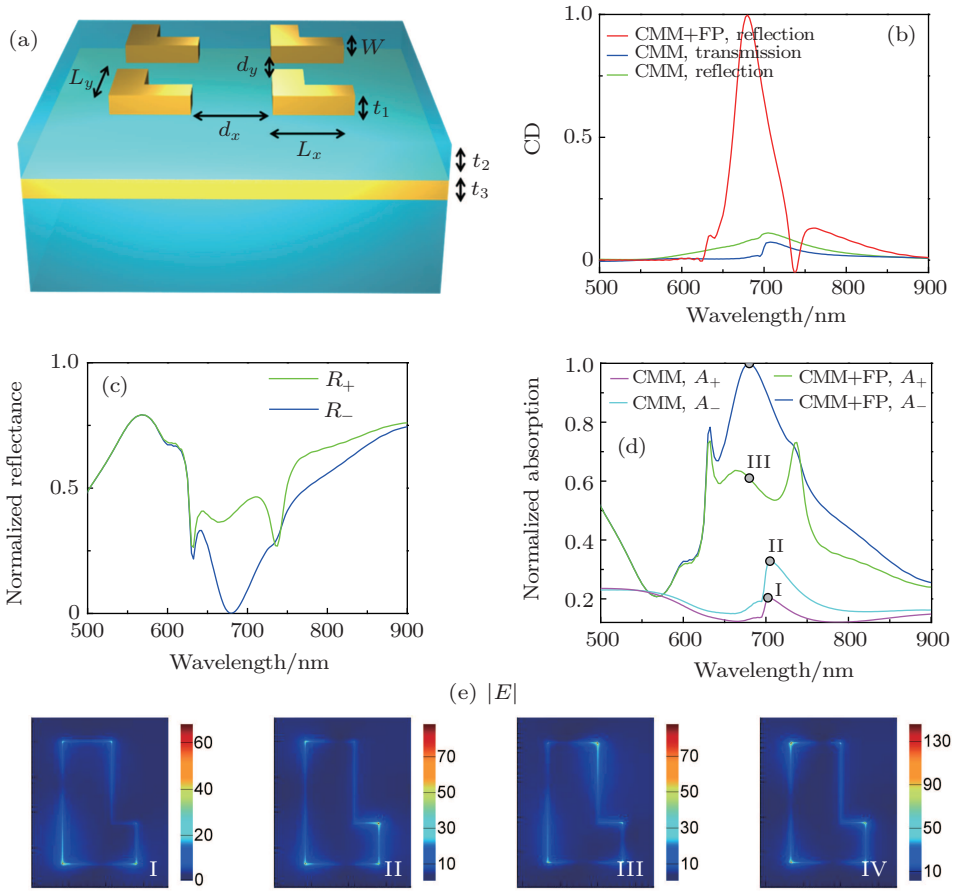


Fig. 1. (color online) Design and simulation results of the FP cavity coupled CMM array. (a) Schematic diagram of proposed cavity structure consisting of a CMM array and a reflector. (b) CD spectra of single CMM array and the FP cavity coupled CMM array. (c) Normal incidence reflectance spectra of the FP cavity coupled CMM. (d) Absorption spectra of single CMM array and the FP cavity coupled CMM array. (e) The magnitudes of electric field $|E|$ of single CMM array (I, II) and the FP cavity coupled CMM (III, IV).

The complex transmission and reflection coefficient can be defined as $E_i = t_{ij}E_j^0$ and $E_i = r_{ij}E_j^0$, where 'i' and 'j' are the polarization states for the RCP (+) and LCP (–) respectively. Corresponding normalized transmission and reflection efficiency can be found from $T_{ij} = |t_{ij}|^2$ and $R_{ij} = |r_{ij}|^2$. The total transmittance and reflectance for the RCP or LCP incidence are denoted as $T_j = T_{jj} + T_{ij}$ and $R_j = R_{jj} + R_{ij}$, respectively. Based on this, the absorption is defined as $A_j = 1 - T_j - R_j$.

CD can be expressed as the difference in transmittance, reflectance, absorption,[6] or extinction cross section[21] between LCP and RCP. In our design, as the transmittance is almost zero, we are mainly concerned with the CD of reflectance which is calculated from

$$\mathrm{CD} = \frac{R_+ - R_-}{R_+ + R_-}. \tag{1}$$

Figure 1(b) shows the simulated results of the CD spectra from the single layer CMM and the FP cavity coupled CMM array (CMM + FP). It is shown that the CD signal from the single layer CMM is relatively weak, where the maximum value is 0.1109 and appears in the reflection spectrum at wavelength 705 nm. Sharing the same plasmonic resonance, the CD spectrum of cavity coupled system is similar to the single layer CMM, but exhibits a dramatically enhanced CD (0.9977) at wavelength 680 nm compared with the single layer CMM (0.07352 in transmittance and 0.1109 in reflection). The CD is enhanced by about nine times via the multi-amplifying mechanism between the two layers. The corresponding reflection components for LCP and RCP for the cavity coupled system are shown in Fig. 1(c). At the resonant wavelength, the normalized reflection of LCP is 0.0004, while the RCP is 0.3901, thus the LCP reflection is efficiently suppressed, showing an extinction ratio about 30 dB.

The comparison of absorption efficiency between the double layer and the single layer is shown in Fig. 1(d). The maximum absorption from the single layer CMM is 0.2038 ($\lambda = 702.5$ nm, point I) of the RCP incidence, which is smaller than the absorption of the LCP incidence (0.328, $\lambda = 705$ nm, point II). Nevertheless, after adding the reflector layer, the normalized absorption of the LCP incidence is dramatically amplified to 0.9996 ($\lambda = 680$ nm, point IV), while the absorption of the RCP incidence is only enhanced to 0.6099 ($\lambda = 680$ nm, point III). The enhancement factors of the absorption efficiencies are both approximately three, meaning the amplification effects of the Fabry–Perot resonance for the absorption are almost the same for both kinds of incident polarizations. The difference in absorption efficiency between the LCP and RCP incidences is also enhanced about three times (from 0.1242 to 0.3897). The above fact shows that the Fabry–Perot resonance does not induce any CD signal, instead, it only amplifies the intrinsic CD signal from the CMM layer. The electric field distributions for these four points indicated in Fig. 1(d) are shown in Fig. 1(e). Comparing III and IV with I and II, it can be seen that the electric field near the L-shaped meta-atom is enhanced after the gold reflector has been added, thus the absorption of cavity coupled CMM is magnified.

Although CD = 1 means that one circular polarization is absorbed completely by the structure, for another polarization, the co- and cross-polarization components may coexist, which is usually not wanted in application. Indeed, the coexistence of co- and cross-polarization components is common in the 2D CMMs except for those structures which are highly symmetric (for example, C_4-symmetric).[22–24] The structure in our design is clearly anisotropic (not C_4 symmetric), thus the corresponding reflection efficiencies should be noticed.

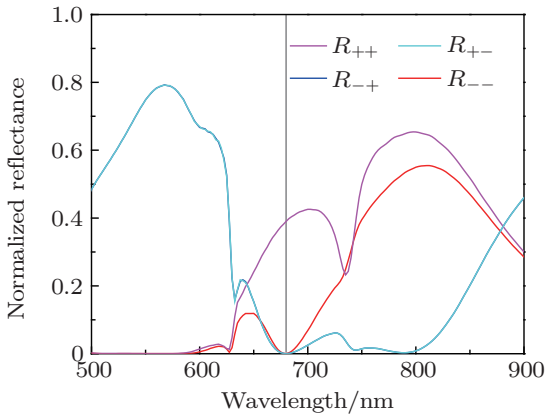


Fig. 2. (color online) Spectra of reflection efficiencies.

Figure 2 shows the co-polarized components R_{++} and R_{--} correspondent to the reflectance of RCP-to-RCP/LCP-to-LCP), and cross-polarized components R_{+-} and R_{-+} corresponding to the reflectance of RCP-to-LCP/ LCP-to-RCP. The vertical gray line denotes the resonant wavelength 680 nm. It is revealed that only the component R_{++} is nonzero at this wavelength, while the other three reflected elements are completely suppressed, indicating that only RCP-to-RCP is allowed to be reflected in our structure, which guarantees that our chiral structure can be used as a polarization device. As the two cross-polarized components are identical, the chirality originates from the difference in the co-polarized element, thus the giant chirality of our structure is based on the intrinsically 2D chiral reflectance effect which is different from the intrinsic 3D chirality.[7,22–24] Additionally, we also investigate the situation under oblique incidence. The cavity coupled chiral structure is stable for the variation in incident angle if the angle with respect to the z axis is less (which is not shown here). Thus our method is suitable for polarization control or other applications.

2.2. Cavity coupling influence

As the tailoring ability of FP cavity is from the radiation coupling[25] dependent on the cavity length, we present the reflection efficiency as a function of incident wavelength and spacer thickness n Fig. 3 to clearly see the influence of FP mode.

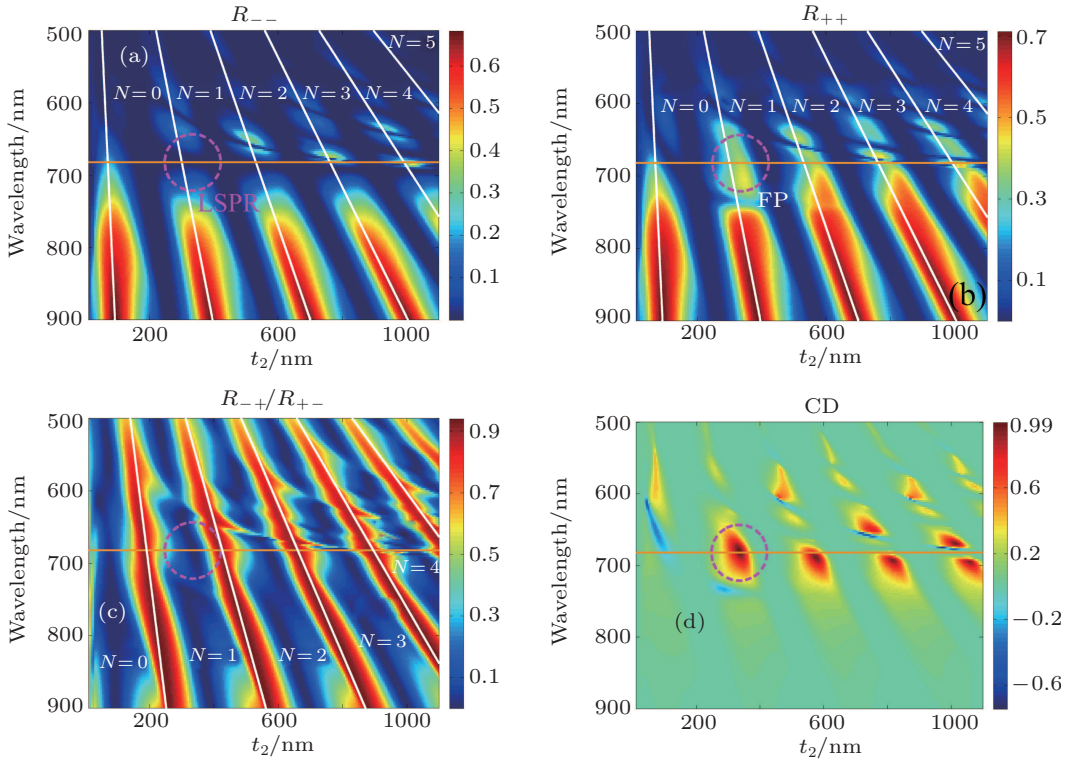


Fig. 3. (color online) Normalized spectra of the reflection efficiencies each as a function of incident wavelength and cavity length for R_{--} (a), R_{++} (b), R_{+-}/R_{-+} (c), white solid and orange lines represent the FP cavity mode and LSPR mode respectively. The purple circle indicates the design in the previous section. (d) CD spectra each as a function of incident wavelength and cavity length.

The values of normalized efficiency R_{--}, for the thickness values of spacer spanning from 10 nm to 1100 nm are first studied in Fig. 3(a). It is shown that this co-polarized component becomes evident when the wavelength is larger than 600 nm. A discrete set of maximum reflection stripes is observed due to the constructive interference in the cavity. FP modes are highlighted (white solid lines) by fitting the FP mode formula as follows:[25–28]

$$2k_0 n_d t_2 - \varphi_B - \varphi_T = 2N\pi, \tag{2}$$

where k_0 is the wave vector in the cavity, n_d is the index of the spacer, φ_B and φ_T are the additional reflection phases from the back mirror and the top CMMs, respectively, and is an integer denoting the order of the resonance ($N = 0, 1, 2, 3, 4, \ldots$). This formula indicates the weak absorption for the efficiency R_{--}. Corresponding order is also marked. Moreover, we observe that there is a region near the wavelength 680 nm where the FP mode vanishes. This is the consequence of a strong excitation of LSPR mode (highlighted by the horizontal orange line) which leads to the normalized reflectance being totally suppressed.

The efficiency R_{++} (in Fig. 3(b)) has a similar pattern to the R_{--}. However along the region of wavelength 680 nm, the LSPR is not so strong that the normalized reflectance is not totally suppressed, but shows periodic variation. Thus chiral phenomena are present for the co-polarization part and will change periodically as a function of spacer thickness. Because the efficiency R_{--} is eliminated, the difference between R_{++} and R_{--} is maximized when R_{++} reaches its peak.

As R_{-+} equals R_{+-}, they have no contribution to the CD and are shown in Fig. 3(c). The white solid lines are also plotted, denoting FP modes. Between these lines the destructive interference condition is satisfied. The reflection efficiencies in Fig. 3(c) are continuous as a function of wavelength, without a horizontal perturbation, indicating that the LSPR is absent for the cross component.

The CD septum is shown Fig. 3(d), where discrete huge CD points near the LSPR wavelength are clearly seen. This huge CD repeats periodically (nearly 225 nm). The aforementioned structure design ($t_2 = 325$ nm) in Fig. 1 is highlighted by the purple circle. For certainty of analysis, this purple circle is also plotted in each of Figs. 3(a)–3(c).

As described above, near the purple circle, the efficiency R_{--} is zero due to the enhanced LSPR, while R_{++} is at the maximum due to the constructive interference. Additionally, the destructive interference condition is satisfied for the cross polarization component. So, according to formula (1), a huge CD value close to 1 is obtained. In a word, due to the different situation for each reflection efficiency, only R_{++} is left outside the cavity, indicating that a circular polarizer which can only reflect RCP light without changing its polarization is realized. Similarly, a polarizer which can only reflect LCP light can be realized if we reverse the "L" particle to its mirror image.

The peculiar dips in Figs. 3(a)–3(d) originate from the higher diffraction order in the cavity.[26] When the normal incident light passes through the CMM, the higher diffraction order is present if the dispersion equation $m(2\pi/P) \leq k_0 n_d$ is

satisfied (m is an integer and P is the lattice period). According to this formula, for the 500-nm incident wavelength the first diffraction order is present in the dielectric spacer if P is larger than 342 nm, and it is present in the air if P is larger than 500 nm. Due to the large lattice period in the y direction (480 nm) the first diffraction order appears only in the cavity. These diffractions can be eliminated by reducing lattice spacing, but at the expense of lowering the chiral response as shown later.

2.3. Asymmetric behavior of the chiral response

In this part, we numerically study the role of lattice spacing in the chiral response. The lattice arrangement is important for the CMMs as the chiral response can be induced for the achiral arrays by appropriately selecting lattice parameters.[29] As our structure is asymmetric ($L_x \neq L_y$), we will observe different responses when lattice spacings are changed in different directions.[30]

The response along the y direction is first studied by varying d_y from 20 nm to 280 nm, where the d_x is set to be a constant of 100 nm. In particular, we study the resonance chiral response near the $t_2 = 325$ nm. Thus the resonance CD value, the resonance wavelength, and the spacer thickness at the resonance position are a function of d_y each. The extracted data are shown in Figs. 4(a) and 4(b). A dramatic increase of CD is observed during the increase of d_y, accompanied by a continuous and significant redshift of resonance wavelength, indicating that we can tune the CD spectrum by varying lattice spacings in the y direction. The vertical gray line indicates that the maximum of the CD (0.98) happens at $d_y = 240$ nm. The fast transform of the resonance wavelength hints at an extreme sensitivity to the geometric variation. In Fig. 4(b), the spacer thickness is also increasing to satisfy the FP condition as the resonance wavelength already has a redshift.

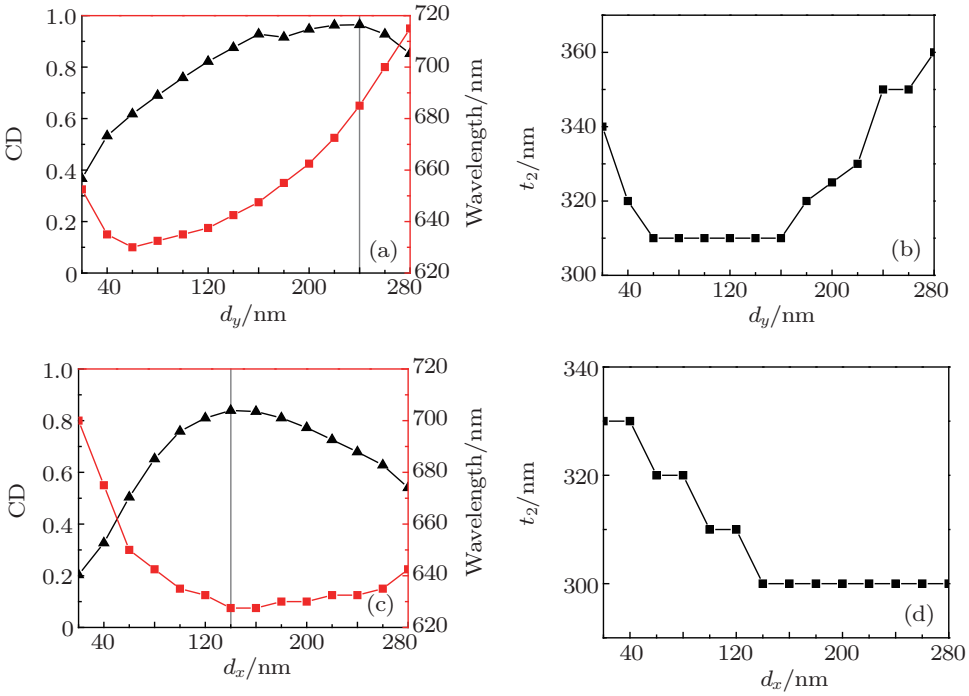


Fig. 4. (color online) Analyses of the role of lattice spacing in chiral response. (a) Extracted resonance CD value, resonance wavelength each as a function of d_y. Vertical gray line indicates the maximum of the CD; (b) extracted spacer thickness at the resonance position as a function of d_y; (c) extracted resonance CD value, resonance wavelength each as a function of d_x, vertical gray line indicates the maximum of the CD; (d) extracted spacer thickness values at the resonance position as a function of d_x.

The role of periodicity along the x direction is also studied in Figs. 4(c) and 4(d) where the d_y is set to be a constant of 100 nm. As shown, the maximum CD is 0.8394 nm at 140-nm wavelength, which is smaller than that in Fig. 4(a). The chiral response transforms rapidly when dx increases from 20 nm to 100 nm, and remains the same in a range from 120 nm to 280 nm. Thus the response of the CMM is stable when d_x is larger than 100 nm. Again we can see it remains unchanged when $d_x > 140$ nm in Fig. 4(d).

From the above analysis, we can see that large d_y is needed to obtain a strong chiral response, and the lattice parameters provide us with an additional degree of freedom for tuning chirality.

We provide the CD spectrum as a function of wavelength and spacer thickness in Fig. 5 to observe the asymmetric behavior of lattice spacing more clearly. As shown in the figure, the maximum of the CD spectrum for $d_x/d_y = 100$ nm/100 nm and $d_x/d_y = 200$ nm/100 nm are 0.851 and 0.78 respectively, and the resonance wavelengths are nearly the same (635 nm and 630 nm), which is in accord with the above analysis. The CD spectrum for $d_x/d_y = 100$ nm/200 nm in Fig. 5(c) has a dramatic increase of the CD strength (0.98) due to the large d_y, but with a down-shifted resonance wavelength (680 nm).

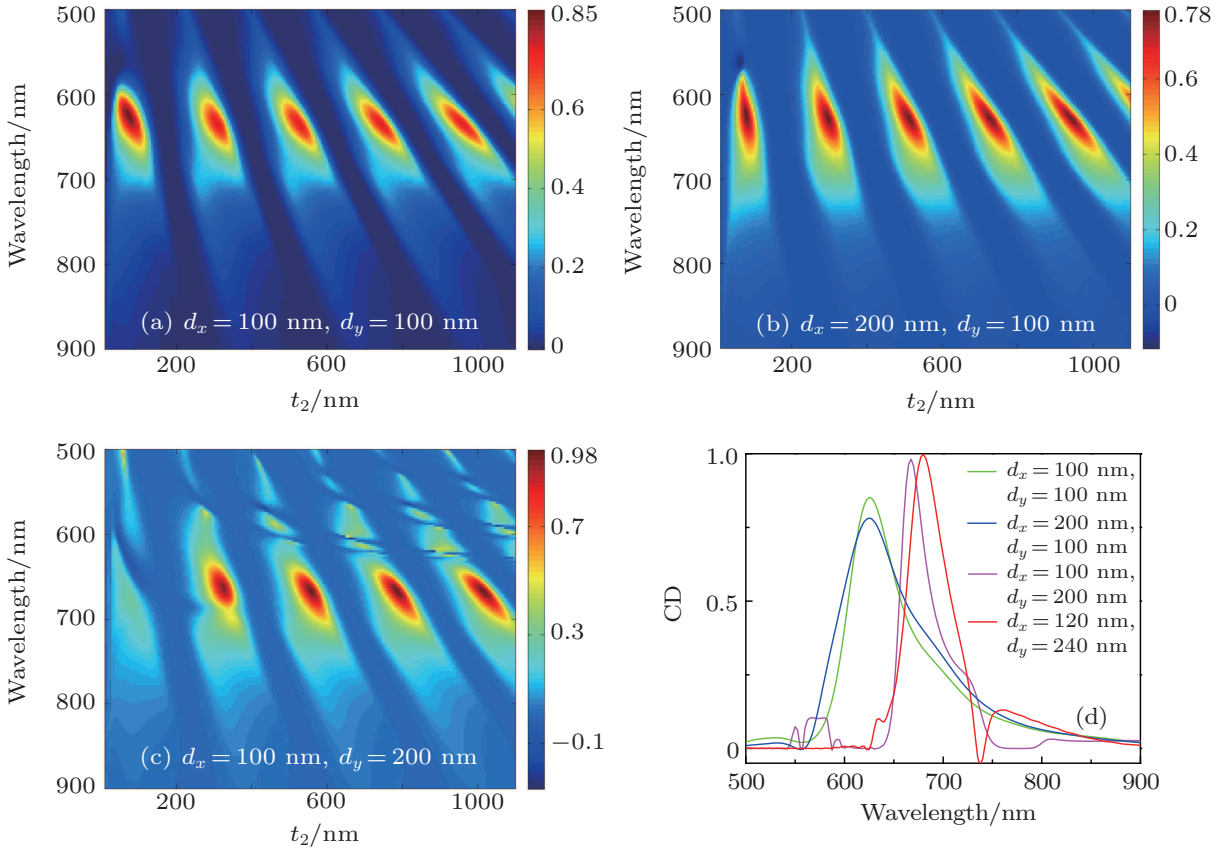


Fig. 5. (color online) Analyses of CD spectra for different geometric parameters: (a) CD spectra as a function of wavelength and cavity length for $d_x/d_y = 100$ nm/100 nm; (b) CD spectra for $d_x/d_y = 200$ nm/100 nm; (c) CD spectra for $d_x/d_y = 100$ nm/200 nm; (d) Extracted maximum CD spectra for the above situations.

The peculiar dips are present only in Fig. 5(c) due to the large lattice period (440-nm along the y direction), which leads to first diffraction order below the CMMs. Meanwhile, for the other situations the lattice period is too small to satisfy the dispersion equation, thus the dips are absent. The extracted maximum CD for the above situations has been plotted in Fig. 5(d) which shows strong CD spectra can be obtained for the larger d_y.

From the analysis of the lattice spacing, we can see two things. The first thing is that to tune the asymmetric MM response effectively, we can start from tuning the in-plane coupling along the direction which significantly affects the chiral response. The second thing is that to obtain a huge CD, how to optimize the parameters (d_x/d_y) is important.

3. Conclusions

In this work, we numerically demonstrate that a huge 2D chiroptical response in the visible band can be obtained by combining the advantages of Fabry–Perot microcavities and 2D CMMs array. The analysis of reflection efficiencies demonstrates that our design can be used as a circular polarization device which can reflect one circular polarization without changing its handedness, and absorb the other. The method of the cavity enhanced chiral response is general. The asymmetric behavior as a function of direction is studied. This analysis also demonstrates an additional degree of freedom for tuning the chirality of asymmetric MMs via varying lattice parameters. Moreover, our design can ease the fabrication requirements such as the precise alignment and high cost in the multi layer MMs.

References

[1] Shi H Y, Li J X, Zhang A X, Wang J F and Xu Z 2014 *Chin. Phys. B* **23** 118101
[2] Liu D Y, Luo X Y, Liu J J and Dong J F 2013 *Chin. Phys. B* **22** 124202
[3] Cao T, Zhang L, Simpson R E, Wei C and Cryan M J 2013 *Opt. Express* **21** 27841
[4] Mutlu M, Akosman A E, Serebryannikov A E and Ozbay E 2011 *Opt. Lett.* **36** 653
[5] Decker M, Zhao R, Soukoulis C M, Linden S and Wegener M 2010 *Opt. Lett.* **35** 1593
[6] Zhao Y, Belkin M A and Alù A 2012 *Nat. Commun.* **3** 870
[7] Cao T, Wei C, Mao L and Li Y 2014 *Sci. Rep.* **4**
[8] Zhang X R, Yang X and Ding X L 2012 *Chin. Phys. B* **21** 093601
[9] Kaschke J, Gansel J K and Wegener M 2012 *Opt. Express 12* **20** 26012
[10] Gansel J K, Thiel M, Rill M S, Decker M, Bade K, Saile V, Freymann G V, Linden S and Wegener M 2009 *Science* **325** 1513
[11] Yang Z Y, Zhao M, Lu P X and Lu Y F 2010 *Opt. Lett.* **35** 2588
[12] McPeak K M, van Engers C D, Blome M, Park J H, Burger S, Gosalvez M A, Faridi A, Ries Y R, Sahu A and Norris D J 2014 *Nano Lett.* **14** 2934
[13] Xu C and Dong J F 2010 *Chin. Opt. Lett.* **8** 1067
[14] Ma W, Kuang H, Xu L, Ding L, Xu C, Wang L and Kotov N A 2013 *Nat. Commun.* **4** 2689
[15] Zhao R, Zhou J, Koschny T, Economou E N and Soukoulis C M 2009 *Phys. Rev. Lett.* **103** 103602

[16] Park H S, Kim T T, Kim H D, Kim K and Min B 2014 *Nat. Commun.* **5** 5435
[17] Ye W, Yuan X, Guo C, Zhang J, Yang B, Liu K, Zhu Z H and Zeng C 2014 arXiv: **1410** 2656
[18] Luo H, Ling X, Zhou X, Shu W, Wen S and Fan D 2011 *Phys. Rev. A* **84** 033801
[19] Wang H and Zhang X 2011 *Phys. Rev. A* **83** 053820
[20] Johnson P B 1972 *Phys. Rev. B* **6** 4370
[21] Hentschel M, Ferry V E and Alivisatos A P 2015 *ACS Photon.* **2** 1253
[22] Wu L, Yang Z Y, Cheng Y Z, Lu Z Q, Zhang P Z, Zhao M Z, Gong R Z, Yuan X H, Zheng Y and Duan J A 2013 *Opt. Express* **21** 5239
[23] Fedotov V A, Mladyonov P L, Prosvirnin S L, Rogacheva A V, Chen Y and Zheludev N I 2006 *Phys. Rev. Lett.* **97** 167401
[24] Plum E 2010 "Chirality and metamaterials", Doctoral Dissertation (University of Southampton) pp. 86–126
[25] Taubert R, Ameling R, Weiss T, Christ A and Giessen H 2011 *Nano Lett.* **11** 4421
[26] Vázquez-Guardado A, Safaei A, Modak S, Franklin D and Chanda D 2014 *Phys. Rev. Lett.* **113** 263902
[27] Bahramipanah M, Dutta-Gupta S, Abasahl B and Martin O J 2015 *ACS Nano* **9** 7621
[28] Zhang B, Zhao Y, Hao Q, Kiraly B, Khoo I C, Chen S and Huang T J 2011 *Opt. Express* **19** 15221
[29] Volkov S N, Dolgaleva K, Boyd R W, Jefimovs K, Turunen J, Svirko Y, Canfiled B K and Kauranen M 2009 *Phys. Rev. A* **79** 043819
[30] Yan C and Martin O J 2014 *ACS Nano* **8** 11860